Wavelength Reuse in a UWB Over Fiber System Based on Phase-Modulation to Intensity-Modulation Conversion and Destructive Interferencing

Wentao Cui, *Student Member, IEEE*, Tong Shao, *Member, IEEE*, and Jianping Yao, *Fellow, IEEE, OSA*

***Abstract*—A novel wavelength reuse scheme based on phase-modulation to intensity-modulation (PM-IM) conversion and destructive interferencing using a polarization modulator (PolM) and a fiber Bragg grating (FBG) in an ultra-wideband (UWB) over fiber (UWBoF) system is proposed and experimentally demonstrated. In the proposed scheme, a PolM and an FBG in the central station (CS) are used to generate intensity-modulated impulse UWB signal based on PM-IM conversion. The downstream UWB signal is sent to a base station (BS) over an optical fiber. At the BS, when the principle axis of the polarizer is aligned with one of the two orthogonal states of polarization (SOPs), the downstream UWB signal is received and detected. When the principle axis of the polarizer is oriented at a special angle to one of the two orthogonal SOPs, a clear optical carrier without intensity modulation is generated, which is then reused for upstream UWB data transmission. A theoretical analysis is performed which is verified by an experiment. A bidirectional point-to-point transmission of 1.25 Gb/s UWB signal over 25-km single-mode fiber (SMF) using a single light source from the CS is demonstrated. The receiver sensitivity and the BER performance for both downstream and upstream transmissions are measured.**

***Index Terms*—Fiber Bragg grating (FBG), frequency discriminator, phase modulation to intensity modulation (PM-IM) conversion, polarization modulator (PolM), UWB over fiber (UWBoF), radio over fiber, wavelength reuse.**

I. Introduction

FOR future wireless local-area network (WLAN) and wireless personal-area network (WPAN) applications, it is generally required that the networks have the properties such as low-complexity, low-cost, low-power consumption and high-data-rate wireless connectivity [1]. Due to the very limited spectrum resources available below 10 GHz, the potential of these networks is restricted by the reality of radio system engineering [2]. To meet the increasing demand for high data rate transmission, ultra-wideband (UWB), which shares the spectrum with the existing radio communications systems, is regarded as a promising solution for future wireless access networks [1], [3]–[5]. In 2002, the US Federal Communications Commission (FCC) approved the unlicensed use of a spectrum from 3.1 to 10.6 GHz centered around 7 GHz with a spectrum width of 7.5 GHz for UWB indoor communication devices. The power spectral density (PSD) is limited to -41.3 dBm/MHz. Due to the low PSD, UWB communications can co-exist with other conventional wireless communications with negligible interferences [1], but the transmission distance is limited to a few to tens of meters. To extend the area of coverage and integrate UWB services into fixed wired or wireless communications networks, a solution is to distribute UWB signals over optical fiber, or UWB over fiber (UWBoF) [6].

On the other hand, to make UWBoF systems practical for future commercial deployment, it is desirable to simplify the operation, ease the maintenance and reduce the cost. Therefore, the construction of a simple base station (BS) and the generation of low-cost impulse UWB signals in the central station (CS) are two main tasks when implementing a UWBoF system [7]. Photonic generation and modulation of UWB signals have been extensively investigated [6], [8]. Wavelength reuse for the transmission of narrow-band upstream signals [9]–[20] has also been proposed. Among the various schemes to achieve wavelength reuse, the utilization of a separated optical carrier for uplink connection [9]–[12], injection locking of a Fabry-Pérot laser diode (FP-LD) [13]–[16], and gain-saturation of a reflective semiconductor optical amplifier (RSOA) [17]–[20] have been considered three major solutions and have been widely investigated. For the schemes using a separated optical carrier, the utilization efficiency of the downstream carrier is low and the demodulation of the downstream signal at the BS is complicated and costly. The major limitation of the schemes using an FP-LD and an RSOA is that a tradeoff between the extinction ratios of the downstream and upstream signals always exists, and the modulation depth and the data rate of the downstream signal have strong impact on the performance of the upstream data transmission.

In this paper, a wavelength reuse scheme for UWBoF system based on phase-modulation to intensity-modulation (PM-IM) conversion and destructive interferencing using a polarization modulator (PolM) and a fiber Bragg grating (FBG) is proposed and experimentally demonstrated. In the proposed system, a PolM is modulated by a Gaussian pulse train coded by a pseudorandom bit sequence (PRBS) pattern to produce two complementary phase-modulated signals along the two principal axes. The two phase-modulated signals are PM-IM converted into two intensity-modulated pulse trains at the FBG, in which the

Manuscript received January 30, 2013; revised May 25, 2013, July 03, 2013; accepted July 24, 2013. Date of publication July 31, 2013; date of current version August 14, 2013. This work was supported by the Natural Sciences and Engineering Research Council of Canada (NSERC).

The authors are with the Microwave Photonics Laboratory, School of Electrical Engineering and Computer Science, University of Ottawa, ON K1N 6N5, Canada (e-mail: jpyao@eecs.uOttawa.ca).

Color versions of one or more of the figures in this paper are available online at http://ieeexplore.ieee.org.

Digital Object Identifier 10.1109/JLT.2013.2276115

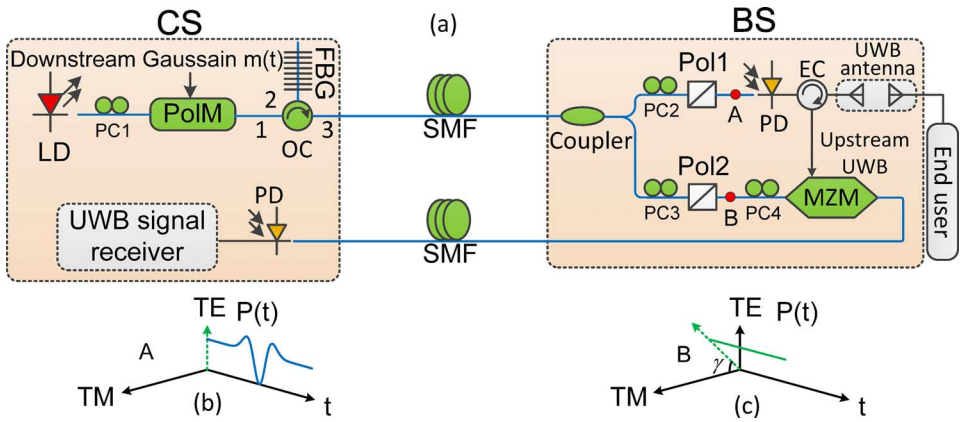

Fig. 1. (a) The proposed UWBoF architecture with wavelength reuse based on a PolM and an FBG. (b) The principle axis of Pol1 is aligned with one SOP (TE) of the incoming signal. (c) The principle axis of Pol1 is aligned with an angle of γ with one SOP (TM) of the incoming signal. EC: electrical circulator, Pol: polarizer.

FBG is used as a frequency discriminator. The downstream signals with intensity modulation on two orthogonal polarization states are sent to a BS through an optical fiber. When the principle axis of the polarizer at the BS is aligned with one of the two orthogonal polarization states, the downstream UWB signal is received and detected. On the other hand, when the principle axis of the polarizer is controlled at a special angle to one of the two orthogonal polarization states, the two projected optical signals on the principle axis of the polarizer would generate two complementary intensity-modulated UWB signals and cancel each other, then a clear optical carrier at the output is generated, and it is reused for upstream UWB data transmission. The proposed wavelength reuse scheme for a UWBoF system has the following advantages. First, a clear optical carrier without intensity modulation for upstream transmission can be generated at the BS, and the erasing process of the downstream data is independent of the modulation depth and data rate of the downstream signal. For the schemes using a separated optical carrier, part of the carriers is not modulated but intended for upstream modulation, the modulation efficiency is thus relatively low. In addition, the demodulation of the subcarrier multiplexed downstream signal at the BS is complicated and costly. In the proposed scheme, the UWB signal is directly generated and modulated on the optical carrier in the optical domain at the CS. At the BS, the upstream service shares exactly the same carrier as the downstream one, which means the optical carrier is completely used for both downstream and upstream services. For the schemes using FP-LDs and RSOAs, there is a tradeoff between the extinction ratios of the downstream and upstream signals, while in the proposed scheme the modulation depth of the downstream signal has negligible impact on the performance of the upstream service. Second, the wavelength reuse at the BS of the proposed system is based on adjusting the principle axis of the polarizer, no active element is utilized. Therefore, there are no additional noise and nonlinearity imposed on the generated optical carrier. This property also contributes to a much clearer optical carrier for upstream transmission. A bidirectional point-to-point transmission of 1.25 Gb/s UWB signal over 25-km single-mode fiber (SMF) is experimentally demonstrated. The performance including the eye diagrams and the bit-error rates (BERs) is evaluated. An error-free transmission of both signals over a 25-km SMF is achieved. A power penalty due to the wavelength reuse is measured to be as low as 0.2 dB.

II. Principle

The schematic of a UWBoF system incorporating our proposed new wavelength reuse scheme is shown in Fig. 1. At the CS, the transceiver consists of a laser diode (LD), a polarization controller (PC), a PolM, an FBG, a photodetector (PD), and a UWB signal receiver. A linearly polarized continuous-wave (CW) light wave emitted from the LD is sent to the PolM through PC1. The PolM is a special phase modulator that supports phase modulations along the two principle axes but with opposite modulation indices. The incident light wave is orientated at an angle of 45° relative to one principle axis of the PolM. Thus, the light wave is projected to the two principle axes with an identical optical power. The PolM is driven by a Gaussian pulse train coded in a PRBS pattern via the radio-frequency (RF) port. Two phase-modulated signals from the PolM are thus generated and sent to the FBG via an optical circulator (OC). When the wavelength of the light wave is located at the linear or quadrature slope of the FBG spectral response, the FBG operates as a frequency discriminator to perform PM-IM conversion. Downstream optical signal from the CS is then sent to the BS through a length of SMF.

At the BS, the received optical signal is divided into two portions. Each portion is sent to a polarizer through a PC (PC2, PC3). By adjusting the principle axis of the polarizer to align with one of the two orthogonal states of polarization (SOPs) of the incoming optical signal, the downstream optical signal can be received. To erase the downstream signal, the principle axis of the polarizer should be tuned to a special angle, thus the carrier can be reused for upstream transmission. As shown in Fig. 1, the upper portion is for the downstream signal transmission. The principle axis of the polarizer (Pol1) is aligned to one of the two orthogonal SOPs of the incoming signal. At the output of Pol1, only the aligned polarization mode is selected while the orthogonally polarized mode is completely attenuated. Then, the optical signal is sent to a PD and the detected electrical

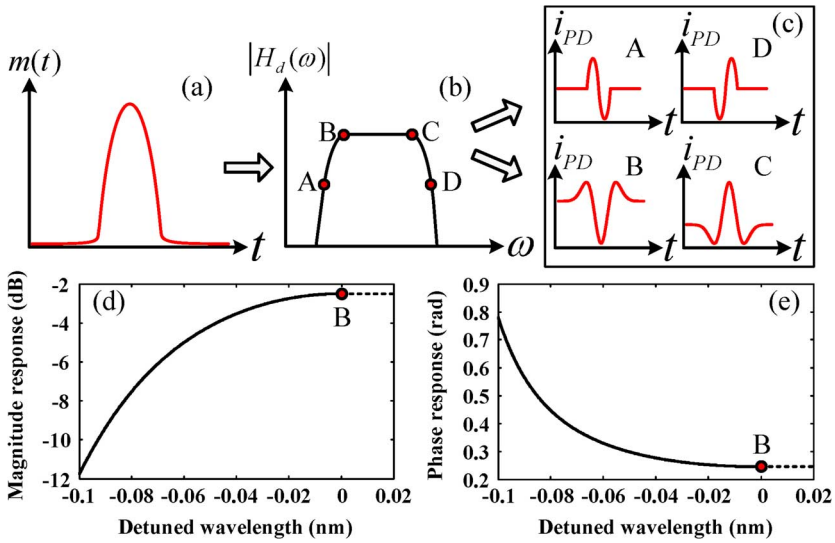

Fig. 2. Reflection spectrum of the FBG-based frequency discriminator and UWB pulse generation based on PM-IM conversion. (a) Temporal waveform of the Gaussian pulse; (b) magnitude response of the FBG-based frequency discriminator; (c) output waveform of the PM-IM converted signals after photodetection; (d) zoom-in view of the magnitude response around point B; (e) zoom-in view of the phase response of the FBG-based frequency discriminator around point B.

UWB signal is radiated to free space via a UWB antenna. A detailed theoretical analysis of the UWB signal generation, transmission and detection will be presented in Section II-A. The lower portion of the optical signal is used for wavelength reuse. As shown in Fig. 1, the principle axis of the polarizer (Pol2) is controlled at a special angle to one of the two orthogonal SOPs of the incoming optical signal. At the output of Pol2, a clear optical carrier without intensity modulation is obtained and is used for upstream transmission. In Section II-B, a detailed theoretical analysis of the signal erasing process will be presented. Then, the generated optical carrier is modulated by an upstream UWB signal at a Mach-Zehnder modulator (MZM) and is used for upstream UWB signal transmission. The upstream signal from the BS is sent to the CS through a length of SMF. At the CS, the optical signal is sent to a PD and then demodulated by a UWB signal receiver.

A. UWB Signal Generation and Detection

At the CS, the key component of the transceiver is the PolM, which is a special phase modulator (PM) that supports both TE and TM modes with opposite phase modulation indices [2]. When the SOP of the linearly polarized CW light is oriented at an angle of 45° relative to one principle axis of the PolM, two complementary phase-modulated signals are generated along the two principal axes [2]. The normalized optical field of the two complementary phase-modulated signals along the two principle axes at the output can be expressed as

$$E_1(t) = \begin{bmatrix} E_{x1}(t) \\ E_{y1}(t) \end{bmatrix} = e^{j\omega_c t} \begin{bmatrix} e^{j\beta m(t)/2} \\ e^{-j\beta m(t)/2} \end{bmatrix}, \quad (1)$$

where ω_c is the angular frequency of the optical carrier, β is the phase modulation index of the PolM, and $m(t)$ is the modulation signal, which is a Gaussian pulse train coded in a PRBS pattern.

The two phase-modulated signals are then sent to the FBG via the OC. When the optical carrier is located at a linear slope of the FBG reflection spectrum, as shown at point **A** or **D** in Fig. 2, the FBG is operating as a linear frequency discriminator where the phase-modulated signal is converted to an intensity-modulated signal. Mathematically, PM-IM conversion in a linear frequency discriminator corresponds to a first-order differentiator [21]. If the modulation signal is a Gaussian pulse, the output signal is a monocycle pulse. On the other hand, when the optical carrier is located at a quadrature slope of the FBG reflection spectrum, as shown at point **B** or **C** in Fig. 2, the FBG also serves as a frequency discriminator, but with a quadratic frequency response, given by

$$H_d(\omega) = [b - K(\omega - \omega_0)^2] + jC. \quad (2)$$

where b, K, and C are constants, and ω_0 is the angular frequency at the maximum of $|H_d(\omega)|$. The optical carrier is set to be at point **B**, as shown in Fig. 2. The values of the parameters mentioned in (2) are given in Table I. By applying the values of all the parameters in (2), the frequency responses in magnitude and

TABLE I
PHYSICAL REPRESENTATIONS AND VALUES OF THE PARAMETERS

Symbol	Physical representation	Value
b	parameter that determines the profile of the FBG reflection spectrum	0.7279
K	parameter that determines the profile of the FBG reflection spectrum	8.8570×10^{-23} (s/rad)
$\lvert\omega_c\text{-}\omega_0\rvert$	frequency detuning of the optical carrier with respect to the peak of the parabola	0 (rad/s)
C	parameter that determines the profile of the FBG reflection spectrum	0.1820
β	phase modulation index of the PolM	0.5928 (rad/V)
$m(t)$	modulation signal: PRBS Gaussian pulse train	1.8 (V) (peak-to-peak amplitude)
$m'(t)$	first-order derivative of the modulation signal	4.3664×10^{10} (V) (peak-to-peak amplitude)
$m''(t)$	second-order derivative of the modulation signal	1.0412×10^{21} (V) (peak-to-peak amplitude)

phase of the FBG based on this theoretical model are plotted at Fig. 2(d) and (e). Then, the signal at the output of the FBG in the frequency domain is given by

$$E_2(\omega) = \begin{bmatrix} E_{x2}(\omega) \\ E_{y2}(\omega) \end{bmatrix} = [b - K(\omega - \omega_0)^2 + jC] \begin{bmatrix} E_{x1}(\omega) \\ E_{y1}(\omega) \end{bmatrix}, \quad (3)$$

where $E_{x1}(\omega)$ and $E_{y1}(\omega)$ are the Fourier transforms of $E_{x1}(t)$ and $E_{y1}(t)$, respectively. $E_{x2}(\omega)$ and $E_{y2}(\omega)$ are the Fourier transforms of the signals at the output of the FBG along the two orthogonal SOPs. Applying the inverse Fourier transform to (3), the signal in the time domain is given by (4), where $E_{x2}(t)$ and $E_{y2}(t)$ are the two PM-IM converted signals along the two orthogonal SOPs; $m'(t)$ and $m''(t)$ are the first- and second-order derivatives of the modulation signal, respectively.

In (4), the angular frequency of the optical carrier ω_c is set to be identical to ω_0, i.e., the input optical carrier is located at the peak point of the parabola in this model. Then, (4) can be rewritten as

$$E_2(t) = \begin{bmatrix} E_{x2}(t) \\ E_{y2}(t) \end{bmatrix} = \begin{bmatrix} b - K(\beta m'(t)/2)^2 + jK\beta m''(t)/2 + jC \\ b - K(\beta m'(t)/2)^2 - jK\beta m''(t)/2 + jC \end{bmatrix} \times \begin{bmatrix} E_{x1}(t) \\ E_{y1}(t) \end{bmatrix}. \quad (5)$$

At the output of port 3 of the OC, the downstream optical signals are generated along the two orthogonal SOPs, as shown in Fig. 1. The optical downstream signals from the CS are transmitted to the BS through a length of SMF.

At the BS, the received optical signal is divided into two portions. Each portion is sent to a PC and a polarizer.

As shown at point A in Fig. 1, the upper portion is for the downstream signal detection. The dotted green line in Fig. 1(b) marks the principle axis of Pol1, which is aligned with one SOP of the incoming signal $E_{y2}(t)$. The signal $E_3(t)$ at the output of the polarizer is expressed as

$$E_3(t) = E_{y2}(t)e^{j\varphi_y}, \quad (6)$$

where φ_y is an additional phase shift introduced to $E_{y2}(t)$ by PC2.

By applying the signal to the PD, a photocurrent is generated which is given by

$$\begin{aligned} i_{PD} &= R|E_3(t)|^2 = R|E_{y2}(t)|^2 \\ &= R|\{[b - K(\beta m'(t)/2)^2] + j[C - K\beta m''(t)/2]\}E_{x1}(t)|^2 \\ &= R\{|[b - K(\beta m'(t)/2)^2] + j[C - K\beta m''(t)/2]||E_{x1}(t)|\}^2 \\ &= R|[b - K(\beta m'(t)/2)^2] + j[C - K\beta m''(t)/2]|^2 \\ &= R\{[b - K(\beta m'(t)/2)^2]^2 + [C - K\beta m''(t)/2]^2\} \\ &= R\left\{ \begin{array}{l} (b^2 + C^2) - [bK\beta^2(m'(t))^2/2 + CK\beta m''(t)] + \\ [K^2\beta^4(m'(t))^4/16 + K^2\beta^2(m''(t))^2/4] \end{array} \right\}, \end{aligned} \quad (7)$$

where R is the responsivity of the PD.

The first and the second terms on the right-hand side in (7) are dc terms. Based on the given values in Table I, the quantitative relationship between the four time-varying terms in (7) is calculated,

$$\left| \frac{bK\beta^2(m'(t))^2/2 + CK\beta m''(t)}{K^2\beta^2(m'(t))^4/16 + K^2\beta^4(m''(t))^2/4} \right| \gg 1. \quad (8)$$

From (8) we can see that the last two terms in (7) are much smaller than the first two time-varying terms and can be ignored. Then, the ac term of the photocurrent is

$$i_{ac} = -R[bK\beta^2(m'(t))^2/2 + CK\beta m''(t)]. \quad (9)$$

The detected signal after the PD is related to the first- and the second-order derivatives of the modulation signal. A simulation is performed to show the shape of the detected downstream pulse. Since the modulation signal is a Gaussian pulse train, the addition of the two terms in (9) leads to a Gaussian-doublet-shaped pulse, as shown in Fig. 3 where a simulated waveform is provided. Therefore, the received electrical UWB signal is a Gaussian doublet pulse train [8].

At the output of the PD, the electrical UWB signal is then radiated to the end users via a UWB antenna. As a result, the link for the downstream UWB service is implemented.

B. Wavelength Reuse for Upstream Transmission

As shown at point B in Fig. 1, the lower portion is for wavelength reuse. When one of the two orthogonal SOPs of the incoming optical signal, say the TM mode, is oriented at an angle

$$\begin{aligned} E_2(t) &= \begin{bmatrix} E_{x2}(t) \\ E_{y2}(t) \end{bmatrix} \\ &= F^{-1}\{[b - K(\omega - \omega_0)^2 + jC]E_1(\omega)\} \\ &= F^{-1}\left\{ \begin{array}{c} bE_1(\omega) - K\omega^2 E_1(\omega) + 2K\omega_0\omega E_1(\omega) \\ -K\omega_0^2 E_1(\omega) + jCE_1(\omega) \end{array} \right\} \\ &= bE_1(t) + KE_1''(t) + \frac{2K\omega_0}{j}E_1'(t) - K\omega_0^2 E_1(t) + jCE_1(t) \\ &= \left\{ \begin{array}{l} b - K[\omega_c - \omega_0 + \beta m'(t)/2]^2 + jK\beta m''(t)/2 + jC \\ b - K[\omega_c - \omega_0 - \beta m'(t)/2]^2 - jK\beta m''(t)/2 + jC \end{array} \right\} \begin{bmatrix} E_{x1}(t) \\ E_{y1}(t) \end{bmatrix} \end{aligned} \quad (4)$$

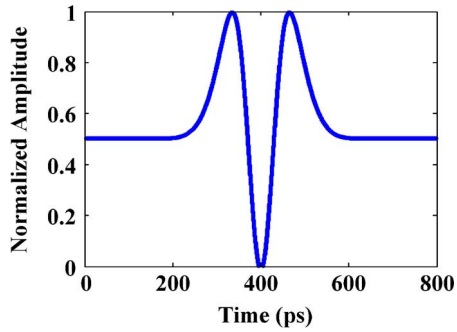

Fig. 3. Detected downstream Gaussian doublet based on PM-IM conversion at the FBG.

of γ to the principle axis of Pol2, as shown in Fig. 1(c), the signal at the output of Pol2 is given by (10), at the bottom of the page, where $\theta_{\rm x}$ and $\theta_{\rm y}$ are the additional phase shifts to $E_{\rm x2}(t)$ and $E_{\rm y2}(t)$ introduced by PC3, respectively, and $\theta_{\rm x}$-$\theta_{\rm y}$ is the phase shift difference between the TE and TM modes.

To obtain a clear optical carrier without any intensity modulation for the upstream transmission, the magnitude of $E_3(t)$ must be a constant, which means

$$|E_3(t)| = \sqrt{E_3(t)\cdot[E_3(t)]^*} = D, \tag{11}$$

where D is a constant.

Substitute (10) into (11), after some mathematical manipulations, we have the following expression for the square of the magnitude of $E_3(t)$

$$\begin{aligned}|E_3(t)|^2 &= E_3(t)\cdot[E_3(t)]^* \\ &= T_1^2 + CK\beta m''(t)\cos(2\gamma) \\ &\quad + T_1^2\sin(2\gamma)\cos\alpha(t) \\ &\quad - T_1\sin(2\gamma)\sin\alpha(t)K\beta m''(t) \\ &\quad + C^2\sin(2\gamma)\cos\alpha(t) + C^2 \\ &\quad + K^2\beta^2(m''(t))^2/4 - K^2\beta^2(m''(t))^2/4 \\ &\quad \cdot\sin(2\gamma)\cos\alpha(t),\end{aligned} \tag{12}$$

where

$$\begin{aligned}T_1 &= b - K(\beta m'(t)/2)^2 \\ T_2 &= C + K\beta m''(t)/2 \\ T_3 &= C - K\beta m''(t)/2 \\ \alpha(t) &= \beta m(t) + \theta_x - \theta_y.\end{aligned} \tag{13}$$

In (12), the term $(K\beta^2 m'(t)^2/4)^2$ in T_1^2 and the term $K^2\beta^2 m''(t)^2/4$ can be neglected since they are very small compared with other terms. Thus (12) is rewritten as

$$\begin{aligned}|E_3(t)|^2 &= E_3(t)\cdot[E_3(t)]^* \\ &= [CK\beta m''(t)\cos(2\gamma) - bK\beta^2(m'(t))^2/2] \\ &\quad + b^2\sin(2\gamma)\cos\alpha(t) - bK\beta^2(m'(t))^2/2 \\ &\quad \cdot\sin(2\gamma)\cos\alpha(t) \\ &\quad - b\sin(2\gamma)\sin\alpha(t)K\beta m''(t) \\ &\quad + C^2\sin(2\gamma)\cos\alpha(t) \\ &\quad + \sin(2\gamma)\sin\alpha(t)K^2\beta^3 m''(t)(m'(t))^2/4 + C^2.\end{aligned} \tag{14}$$

By tuning PC3, $\theta_{\rm x}$-$\theta_{\rm y}$ and γ can be adjusted, which controls the bias point on the cosine transfer function $\cos[\alpha(t)]$ and the value of $\cos(2\gamma)$ and $\sin(2\gamma)$.

When the Gaussian pulse is biased near the maximum or minimum transmission point, owing to the nonlinear nature of the transfer function, the shape of the Gaussian pulse is changed. If the amplitude of the Gaussian pulse is large enough, the pedestal and peak parts of the Gaussian pulse will lie in the complementary slopes of the transfer function, resulting in the generation of a Gaussian doublet [22], as shown in Fig. 4. In the implementation, γ and $\theta_{\rm x}$-$\theta_{\rm y}$ can be controlled by adjusting PC3 to make the Gaussian pulse be nonlinearly shaped into a Gaussian doublet.

In (14), the first two terms represent a Gaussian doublet originating from their complex combination. The last term is a dc term. Therefore, to ensure the square of the magnitude of $E_3(t)$

$$\begin{aligned}E_3(t) &= E_{x2}(t)e^{j\theta_x}\cos(\gamma) + E_{y2}(t)e^{j\theta_y}\sin(\gamma) \\ &= \{[b - K(\beta m'(t)/2)^2] + j[C + K\beta m''(t)/2]\}E_{x1}(t)e^{j\theta_x}\cos(\gamma) \\ &\quad + \{[b - K(\beta m'(t)/2)^2] + j[C - K\beta m''(t)/2]\}E_{y1}(t)e^{j\theta_y}\sin(\gamma) \\ &= [b - K(\beta m'(t)/2)^2]\{E_{x1}(t)e^{j\theta_x}\cos(\gamma) + E_{y1}(t)e^{j\theta_y}\sin(\gamma)\} \\ &\quad + [C + K\beta m''(t)/2]E_{x1}(t)e^{j(\theta_x+\pi/2)}\cos(\gamma) \\ &\quad + [C - K\beta m''(t)/2]E_{y1}(t)e^{j(\theta_y+\pi/2)}\sin(\gamma) \\ &= [b - K(\beta m'(t)/2)^2]\left\{\begin{matrix}e^{j(\omega_c t+\beta m(t)/2+\theta_x)}\cos(\gamma)+\\ e^{j(\omega_c t-\beta m(t)/2+\theta_y)}\sin(\gamma)\end{matrix}\right\} \\ &\quad + [C + K\beta m''(t)/2]e^{j(\omega_c t+\beta m(t)/2+\theta_x+\pi/2)}\cos(\gamma) \\ &\quad + [C - K\beta m''(t)/2]e^{j(\omega_c t-\beta m(t)/2+\theta_y+\pi/2)}\sin(\gamma) \\ &= [b - K(\beta m'(t)/2)^2]e^{j(\omega_c t+\theta_y)}\left[\begin{matrix}e^{j(\beta m(t)/2+\theta_x-\theta_y)}\cos(\gamma)+\\ e^{-j\beta m(t)/2}\sin(\gamma)\end{matrix}\right] \\ &\quad + e^{j(\omega_c t+\theta_y+\pi/2)}\left\{\begin{matrix}[C + K\beta m''(t)/2]e^{j(\beta m(t)/2+\theta_x-\theta_y)}\cos(\gamma)+\\ [C - K\beta m''(t)/2]e^{-j\beta m(t)/2}\sin(\gamma)\end{matrix}\right\},\end{aligned} \tag{10}$$

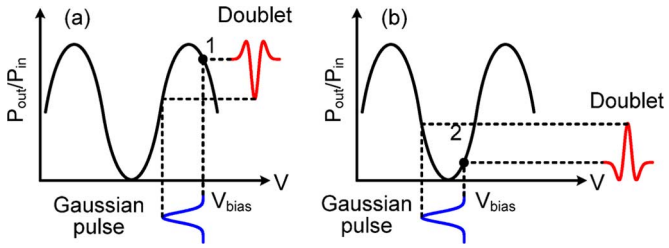

Fig. 4. Principle of UWB doublet generation based on the nonlinear shaping of a Gaussian pulse on a cosine transfer function [22]. (a) Biased near the maximum transmission point. (b) Biased near the minimum transmission point.

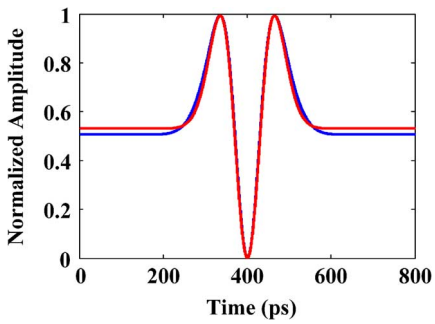

Fig. 5. Simulated waveforms of the generated Gaussian doublets based on complex combination.

to be a constant, the combination of the other terms in (14) should be shaped into a Gaussian doublet with the same shape and amplitude as those of the first two terms, but with the opposite polarity, by adjusting γ and θ_x-θ_y.

Fig. 5 shows the generated Gaussian doublets based on the complex combination in (14). The doublet in blue represents the pulse from the combination of the first two terms in (14); while the red doublet represents that from the combination of the other time-varied terms. Comparing the waveforms in Fig. 5, it is clearly seen that the two doublets have the same pulse shape. In this calculation, the values of the parameters are given in Table I. γ and θ_x-θ_y are adjusted to be 0.5189π and 0.8550π, respectively. In addition, the peak-to-peak amplitudes of the two pulses and their difference are also obtained through the calculation, given by

$$\begin{aligned} Vpp1 &\approx Vpp2 = 0.0134(\mathrm{V}) \\ Vpp1 - Vpp2 &= 3.1501 \times 10^{-5}(\mathrm{V}), \end{aligned} \tag{15}$$

where $Vpp1$ and $Vpp2$ denote the peak-to-peak amplitudes of the two doublets, respectively. The peak-to-peak amplitude difference between the two pulses is small enough. Therefore, we can conclude that two identical Gaussian doublets are generated through such complex combination of different terms. By changing the sign of γ in (14), the polarity of one doublet is inverted, which leads to the complete cancellation of the two pulses. In this situation, the addition of the two doublets generates a dc component, which means the output optical signal from Pol2 is a clear optical carrier with constant intensity, which is suitable for upstream transmission.

Note that the polarization variations during the downstream optical transmission will have impact on the performance of the system. A solution is to use a polarization stabilizer at the BS. The use of a polarization stabilizer to compensate the polarization variations has been proposed and employed in polarization-multiplexed transmission systems [23]. In our proposed system, a polarization stabilizer should be placed at the BS right after the fiber transmission link.

III. Experiment

The proposed wavelength reuse scheme in a UWBoF system is experimentally demonstrated. The experimental setup is shown in Fig. 6. At the CS, a CW light at 1555.02 nm from a tunable laser source (TLS) is applied to a PolM through PC1. The PolM (Versawave Technologies) is driven by a 1.25-Gb/s Gaussian pulse train coded in a $2^{15} - 1$ PRBS pattern, generated by a bit error rate tester (BERT, Agilent 4901B). The optical signal at the output of the PolM is then amplified by an erbium-doped fiber amplifier (EDFA1) and sent to an FBG through an OC. The FBG is used as a frequency discriminator which has a center wavelength of 1556.08 nm and a reflectivity greater than 90%. In the experiment, the wavelength of the optical carrier is controlled to be located at the left quadrature slope of the FBG reflection spectrum. Therefore, a Gaussian doublet pulse train is generated at the output of the FBG. The FBG is placed after EDFA1 to also filter out the noise induced by EDFA1. The intensity-modulated downstream UWB signal is then transmitted through a 25-km SMF (Corning SM28) to the BS. At the BS, the downstream optical signal is divided into two portions by an optical coupler. In the upper portion, the downstream UWB signal is received when the principle axis of the polarizer (Pol1) is aligned with one of the two orthogonal SOPs and then sent to a 25-GHz PD. To further block the noise, a high pass filter (HPF) with a cutoff frequency of 3-GHz is utilized after the PD. Then, the electrical UWB signal is demodulated by a UWB receiver. The details of the UWB receiver will be presented at the end of this Section. In the lower portion, a clear optical carrier without intensity modulation is generated when the principle axis of the polarizer (Pol2) is oriented at a special angle relative to one of the two orthogonal SOPs of the incoming optical signal, as indicated in (14). Then, the clear optical carrier is amplified by EDFA2 and then applied to an MZM through PC4 where it is modulated by an upstream UWB signal. The upstream UWB signal is a 1.25-Gb/s UWB monocycle pulse train coded in a $2^{15} - 1$ PRBS pattern, generated by an arbitrary waveform generator (AWG, Tektronix AWG 7102). The upstream optical signal is transmitted back to the CS through a 25-km SMF. At the CS, the upstream optical signal is converted to an electrical signal at a 25-GHz PD and then sent to a UWB receiver. The performance of both downstream and upstream signal transmissions in the wavelength reused system is evaluated by measuring the eye diagrams and the bit error rates of the transmitted signals.

Due to the unavailability of a UWB correlation receiver, a UWB receiver using a mixer, a structure similar to what we used in [24], [25] is utilized, as shown in Fig. 7. At the output of the PD, the UWB signal is first amplified by a wideband electrical amplifier (AMP1, 23-dB gain) and then applied to the mixer to mix with a local oscillator (LO) signal at 6.25 GHz. At the output of the mixer, the UWB signal is converted to a baseband signal which is amplified by a second wideband amplifier

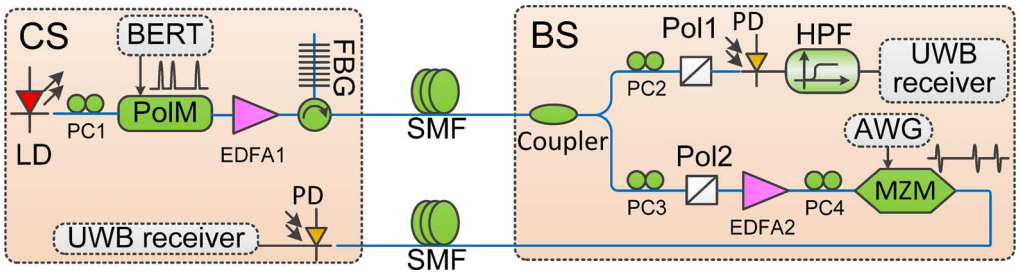

Fig. 6. Experimental setup of the wavelength reused UWBoF system.

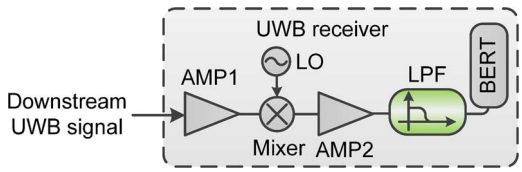

Fig. 7. A UWB receiver used in the experiment.

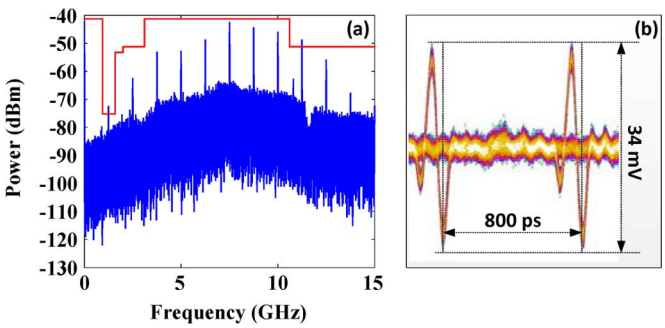

Fig. 8. (a) Measured electrical spectrum and (b) measured eye diagram of the received downstream UWB signal.

(AMP2, 10-dB gain), filtered by a low-pass filter (LPF) with a cutoff frequency of 1.2 GHz, and sent to the BERT.

At the CS, the wavelength of the CW light from the TLS is tuned to be located at the left quadrature slope of the FBG reflection spectrum. At the BS, the HPF not only blocks the noise, but also exhibits a differential effect on the input UWB signal due to the high pass characteristics. Therefore, the received electrical UWB doublet pulse after the HPF becomes a Gaussian triplet. The eye diagram as well as the electrical spectrum of the received UWB signal is measured and shown in Fig. 8. As can be seen the eyes of the received downstream UWB signal are both widely opened. In addition, the PSD of the UWB signal meets the FCC spectrum mask for indoor wireless communication as well.

In the lower portion, by tuning the polarization direction via adjusting PC3, a clear optical carrier for upstream transmission is generated at the output of Pol2. To show the data erasing performance, we measure the temporal waveforms of the optical carrier at the output of Pol2 after photodetection when the downstream signal does not carry and carry data information. As shown in Fig. 9, the waveforms with or without data information are identical, indicating that the data information is completely erased. The effectiveness of the data erasing is verified. The clear optical carrier is then used for upstream signal transmission.

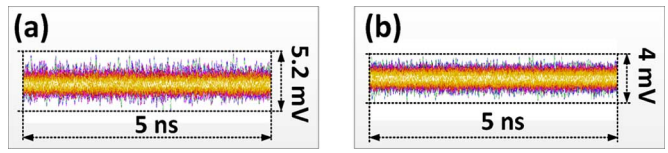

Fig. 9. The temporal waveform after photodetection when (a) the downstream signal does not carry data information, (b) the downstream signal carries data information, but the data is erased.

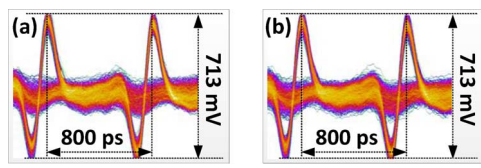

Fig. 10. Measured eye diagrams of the received upstream UWB signals. (a) Without a downstream UWB signal, (b) with a downstream UWB signal.

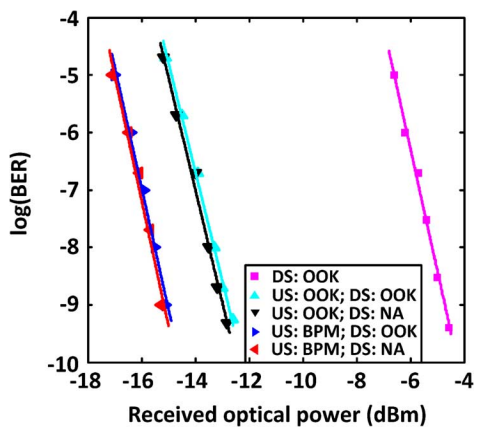

Fig. 11. BER measurements of the upstream UWB signals with and without a downstream signal. US: upstream, DS: downstream.

The generated optical carrier at the output of the polarizer has a power of −2 dBm and it is amplified by EDFA2. The power at the output of EDFA2 is 5 dBm. Fig. 10 shows the measured eye diagrams of an on-off-keying (OOK) modulated UWB upstream signal with or without a downstream UWB signal. The eyes for the two cases with or without a downstream UWB signal are widely open, no obvious deterioration is observed for the eye diagram shown in Fig. 10(b). This confirms again the effective data erasing process and the good performance of the wavelength reuse scheme.

Fig. 11 shows the BER measurements of the downstream signal and upstream signals with and without a downstream

TABLE II
POWER BUDGET OF THE PROPOSED UWB OVER FIBER SYSTEM

Downstream service		**Upstream service**	
Minimum required power at BS	**1 dBm**	**Upstream receiver sensitivity**	**-15.1 dBm**
Downstream receiver sensitivity	-5 dBm	Loss at MZM	8 dB
Loss at Pol1	3 dB	Fiber transmission and connecter loss	6 dB
Loss at coupler	3 dB	Minimum upstream optical carrier power before MZM	-1.1 dBm
Fiber transmission loss	5 dB		
Loss of other connecters	1 dB	EDFA2 output power	5 dBm
Minimum launch power from CS	**7 dBm**	**Power margin**	**6.1 dB**

UWB signal. Error free transmission for a downstream UWB signal and an OOK or bi-phase modulation (BPM) upstream UWB signal with or without a downstream modulation is achieved. Error free transmission here is defined as the transmission of a signal with a BER no more than 10^{-9}. As can be observed from the BER measurements, the power penalty induced due to the existence of a downstream UWB modulation is less than 0.2 dB. In addition, the BER performance of the UWB transmission based on BPM is better than that based on OOK, providing about 2 dB additional power margin. This is because the electrical power of a BPM modulated UWB signal is 3 dB greater than that of an OOK modulated UWB signal. The receiver sensitivities for the OOK downstream transmission, OOK and BPM upstream transmission with a downstream UWB modulation are -5 dBm, -13 dBm and -15.1 dBm, respectively. The receiver sensitivity here is defined as the optical power to obtain a BER of 10^{-9} for the UWB signal receiver. The receiver sensitivity of the downstream transmission is relatively low compared with that of the upstream transmission; this is because the effective modulation depth of the downstream UWB signal is reduced after the PM-IM conversion. The receiver sensitivity of the UWB downstream transmission can be enhanced by using an FBG with a higher reflectivity and a larger slope at the linear region of the reflection spectrum profile. In addition, it should be noted that the receiver sensitivity of both the UWB downstream and upstream transmission can be enhanced if a UWB correlation receiver with low noise pre-amplifiers is utilized.

The power budget of the proposed UWBoF system is evaluated and given in Table II, based on the investigation of the optical receiver sensitivities for both the downstream and upstream transmission. In Table II, the powers needed at the downstream and upstream receivers are presented. If the downstream EDFA (EDFA1) is eliminated, and the LD output power is increased to 16 dBm, the output power from the CS will be 5 dBm (where the losses induced by the PolM and the FBG are 4 dB and 7 dB, respectively). The maximum attainable transmission distance is $(5-1)/0.2 = 20$ km. If the upstream EDFA (EDFA2) is eliminated, after 20-km SMF transmission, the optical power after Pol2 is -2 dBm, the output power from the BS is -10 dBm, and then the maximum transmission distance for the upstream service is $[(-10-1)-(-15.1)]/0.2 = 20.5$ km. The downstream and upstream transmission distances are very close. In this experiment, since the SMF has a fixed length of 25 km, therefore, optical amplification is used. In addition, the employment of the EDFAs enables the system to have a higher power margin and reduces the requirement for a high power laser source at the CS.

In addition, since there is no light source at the BSs, an optical amplifier is required to compensate the loss induced by the downstream and upstream links. This optical amplifier (an EDFA, for example) can be placed at the remote access node and shared by multiple BSs. Moreover, the optical power required at the BS is calculated based on the measured optical receiver sensitivity in our experimental setup. We would expect that the requirement of the optical power launched into the downstream/upstream fiber link can be significantly reduced by alternatively using low-noise amplifiers at the optical receivers in both the CS and BS.

IV. CONCLUSION

A wavelength reuse scheme based on PM-IM conversion and destructive interferencing in a UWBoF system was proposed and experimentally demonstrated. The key contribution of the technique was the use of the PolM which was operating jointly with the FBG to generate intensity-modulated downstream UWB signal based on PM-IM conversion. The combination of the two orthogonal signals at a polarizer would generate a clean optical carrier which was reused for upstream transmission. In addition, since no active elements are employed in the downstream signal erasing process, no additional noise and nonlinearity are introduced, and the quality of the upstream signal is thus greatly enhanced. A bidirectional point-to-point transmission of 1.25 Gb/s UWB signal over 25-km SMF was achieved. The performance including the eye diagrams and the BERs was evaluated. An error-free transmission over a 25-km SMF was demonstrated.

REFERENCES

[1] G. R. Aiello and G. D. Rogerson, "Ultra-wideband wireless systems," *IEEE Microw. Mag.*, vol. 4, no. 2, pp. 36–47, Jun. 2003.
[2] S. Pan and J. Yao, "IR-UWB-over-fiber systems compatible with WDM-PON networks," *J. Lightw. Technol.*, vol. 29, no. 20, pp. 3025–3034, Oct. 2011.
[3] D. Porcino and W. Hirt, "Ultra-wideband radio technology: Potential and challenges ahead," *IEEE Commun. Mag.*, vol. 41, no. 7, pp. 66–74, Jul. 2003.
[4] M. Ghavami, L. B. Michael, and R. Kohno, *Ultra Wideband Signals and Systems in Communication Engineering*. West Sussex, U.K.: Wiley, 2004.
[5] I. Oppermann, M. Hämäläinen, and J. Iinatti, *UWB Theory and Applications*. Chichester, U.K.: Wiley, 2004.
[6] J. P. Yao, F. Zeng, and Q. Wang, "Photonic generation of ultrawideband signals," *J. Lightw. Technol.*, vol. 25, no. 11, pp. 3219–3235, Nov. 2007.
[7] Z. Dong, J. Lu, Y. Pi, X. Lei, L. Chen, and J. Yu, "Optical millimeter-wave signal generation and wavelength reuse for upstream connection in radio-over-fiber systems," *J. Opt. Netw.*, vol. 7, no. 8, pp. 736–743, Aug. 2008.
[8] J. P. Yao, "Photonics for ultrawideband communications," *IEEE Microw. Mag.*, vol. 10, no. 4, pp. 82–95, Jun. 2009.
[9] L. Chen, H. Wen, and S. Wen, "A radio-over-fiber system with a novel scheme for millimeter-wave generation and wavelength reuse for up-link connection," *IEEE Photon. Technol. Lett.*, vol. 18, no. 19, pp. 2056–2058, Oct. 2006.
[10] Z. Jia, J. Yu, and G.-K. Chang, "A full-duplex radio-over-fiber system based on optical carrier suppression and reuse," *IEEE Photon. Technol. Lett.*, vol. 18, no. 16, pp. 1726–1728, Aug. 2006.

[11] A. Kaszubowska, L. Hu, and L. Barry, "Remote downconversion with wavelength reuse for the radio/fiber uplink connection," *IEEE Photon. Technol. Lett.*, vol. 18, no. 4, pp. 562–564, Feb. 15, 2006.
[12] J. Yu, Z. Jia, T. Wang, and G. K. Chang, "A novel radio-over-fiber configuration using optical phase modulator to generate an optical mm-wave and centralized lightwave for uplink connection," *IEEE Photon. Technol. Lett.*, vol. 19, no. 3, pp. 140–142, Feb. 2007.
[13] L. Y. Chan, C. K. Chan, D. T. K. Tong, F. Tong, and L. K. Chen, "Upstream traffic transmitter using injection-locked Fabry-Pérot laser diode as modulator for WDM access networks," *Electron. Lett.*, vol. 38, no. 1, pp. 43–45, Jan. 2002.
[14] W. Hung, C. K. Chan, L. K. Chen, and F. Tong, "An optical network unit for WDM access networks with downstream DPSK and upstream remodulated OOK data using injection-locked FP laser," *IEEE Photon. Technol. Lett.*, vol. 15, no. 10, pp. 1476–1478, Oct. 2003.
[15] F. Xiong, W.-D. Zhong, and H. Kim, "A broadcast-capable WDM-PON based on polarization-sensitive weak-resonant-cavity Fabry-Perot laser diodes," *J. Lightw. Technol.*, vol. 30, no. 3, pp. 355–361, Feb. 2012.
[16] S. M. Lee, K. M. Choi, S. G. Mun, J. H. Moon, and C. H. Lee, "Dense WDM-PON based on wavelength-locked Fabry-Pérot laser diodes," *IEEE Photon. Technol. Lett.*, vol. 17, no. 7, pp. 1579–1581, Jul. 2005.
[17] W. R. Lee, M. Y. Park, S. H. Cho, J. H. Lee, C. Y. Kim, G. Jeong, and B. W. Kim, "Bidirectional WDM-PON based on gain-saturated reflective semiconductor optical amplifiers," *IEEE Photon. Technol. Lett.*, vol. 17, no. 11, pp. 2460–2462, Nov. 2005.
[18] I. Papagiannakis, M. Omella, D. Klonidis, J. A. Lázaro, A. Birbas, J. Kikidas, I. Tomkos, and J. Prat, "Design characteristics for a full-duplex IM/IM bidirectional transmission at 10 Gb/s using low bandwidth RSOA," *J. Lightw. Technol.*, vol. 28, no. 7, pp. 1094–1101, Apr. 2010.
[19] T. Y. Kim and S. K. Han, "Reflective SOA-based bidirectional WDM-PON sharing optical source for up/downlink data and broadcasting transmission," *IEEE Photon. Technol. Lett.*, vol. 18, no. 22, pp. 2350–2352, Nov. 15, 2006.
[20] M. Presi, R. Proietti, K. Prince, G. Contestabile, and E. Ciaramella, "A 80 km reach fully passive WDM-PON based on reflective ONUs," *Opt. Exp.*, vol. 16, no. 23, pp. 19043–19048, Nov. 2008.
[21] Q. Wang and J. P. Yao, "An electrically switchable optical ultra-wideband pulse generator," *J. Lightw. Technol.*, vol. 25, no. 11, pp. 3626–3633, Nov. 2007.
[22] Q. Wang and J. P. Yao, "UWB doublet generation using a nonlinearly-biased electro-optic intensity modulator," *Electron. Lett.*, vol. 42, no. 22, pp. 1304–1305, Oct. 2006.
[23] P. Boffi, M. Ferrario, L. Marazzi, P. Martelli, P. Parolari, A. Righetti, R. Siano, and M. Martinelli, "Measurement of PMD tolerance in 40-Gb/s polarization-multiplexed RZ-DQPSK," *Opt. Express*, vol. 16, no. 17, pp. 13398–13404, Aug. 2008.
[24] S. Pan and J. P. Yao, "Simultaneous provision of UWB and wired services in a WDM-PON network using a centralized light source," *IEEE Photon. J.*, vol. 2, no. 5, pp. 711–718, Oct. 2010.
[25] S. Pan and J. P. Yao, "A UWB over fiber system compatible with WDM-PON architecture," *IEEE Photon. Technol. Lett.*, vol. 22, no. 20, pp. 1500–1502, Oct. 15, 2010.

Wentao Cui received the B.Eng. degree in electrical engineering from Tianjin University, Tianjin, China, in 2011.

Since September 2011, he has been a Master of Applied Science Student with the Microwave Photonics Research Laboratory, School of Electrical Engineering and Computer Science, University of Ottawa, Ottawa, ON, Canada. His research interests include photonic generation of Ultra-Wide-Band signal, wavelength division multiplexed passive optical networks and ultra-wideband over fiber technology.

Tong Shao received the B.S. and M.S. degrees from Tsinghua University, Beijing, China, in 2007 and 2009, respectively, and the Ph.D. degree from Institut National Polytechnique de Grenoble (INP-Grenoble), Grenoble, France, in 2012. He joined the Microwave Photonics Research Laboratory, School of Electrical Engineering and Computer Science, University of Ottawa, as a post-doctoral fellow in August 2012. His current research interests include optical communications, radio over fiber technologies, ultra-wideband over fiber technologies, and microwave photonics.

Jianping Yao (M'99-SM'01-F'12) received the Ph.D. degree in electrical engineering from the Université de Toulon, France, in December 1997. He joined the School of Electrical Engineering and Computer Science, University of Ottawa, Ottawa, Ontario, Canada, as an Assistant Professor in 2001, where he became an Associate Professor in 2003, a Full Professor in 2006. He was appointed University Research Chair in Microwave Photonics in 2007. From July 2007 to June 2010, he was Director of the Ottawa-Carleton Institute for Electrical and Computer Engineering. Prior to joining the University of Ottawa, he was an Assistant Professor in the School of Electrical and Electronic Engineering, Nanyang Technological University, Singapore, from 1999 to 2011.

Dr. Yao has published more than 410 papers, including more than 230 papers in peer-reviewed journals and 180 papers in conference proceedings. He is a Chair of numerous international conferences, symposia, and workshops, including the Vice-TPC Chair of the 2007 IEEE Microwave Photonics Conference, TPC Co-Chair of the 2009 and 2010 Asia-Pacific Microwave Photonics Conferences, TPC Chair of the high-speed and broadband wireless technologies subcommittee of the 2009–2012 IEEE Radio Wireless Symposia, TPC Chair of the microwave photonics subcommittee of the 2009 IEEE Photonics Society Annual Meeting, TPC Chair of the 2010 IEEE Microwave Photonics Conference, and General Co-Chair of the 2011 IEEE Microwave Photonics Conference. Dr. Yao received the 2005 International Creative Research Award at the University of Ottawa. He was the recipient of the 2007 George S. Glinski Award for Excellence in Research. Dr. Yao was selected to receive an inaugural OSA outstanding reviewer award in 2012. He is an IEEE distinguished microwave lecturer for 2013–2015.

Dr. Yao is a registered Professional Engineer of Ontario. He is a Fellow of the IEEE, a Fellow of the Optical Society of America, and a Fellow of the Canadian Academy of Engineering.